Journal of Advanced Ceramics
2013, 2(1): 42–48
DOI: 10.1007/s40145-013-0040-6 ISSN 2226-4108

Research Article

Thermoelectric performance enhancement of $(BiS)_{1.2}(TiS_2)_2$ misfit layer sulfide by chromium doping

Yulia Eka PUTRI[a], Chunlei WAN[a,b], Ruizhi ZHANG[c], Takao MORI[d], Kunihito KOUMOTO[a,b,*]

[a]*Graduate School of Engineering*, *Nagoya University*, *Nagoya 464-8603*, *Japan*
[b]*CREST*, *Japan Science and Technology Agency*, *Tokyo 102-0075*, *Japan*
[c]*Department of Physics*, *State Key Laboratory of Photoelectric Technology and Functional Materials* (*Culture Base*), *Northwest University*, *Xi'an 710069*, *China*
[d]*National Institute for Materials Science* (*NIMS*), *Tsukuba 305-0044*, *Japan*

Received: December 08, 2012; Revised: January 15, 2013; Accepted: January 16, 2013

Abstract: A misfit layer sulfide $(BiS)_{1.2}(TiS_2)_2$ with a natural superlattice structure has been shown to be a promising thermoelectric material, but its high carrier concentration should be reduced so as to further optimize the thermoelectric performance. However, ordinary acceptor doping has not succeeded because of the non-parabolic band structure. In this paper, we have successfully doped chromium ions into the Ti sites, which can maintain or even enhance the high effective mass of electrons so as to effectively improve *ZT* value. X-ray diffraction analysis, coupled with X-ray photoelectron spectroscopy, shows that chromium has been substituted into titanium sites in TiS_2 layers and confirms its ionic state. The chromium doping has successfully reduced the carrier concentration with the subsequent reduction of electrical conductivity. Unlike other acceptor dopants (alkaline earth metals), chromium also enhances Seebeck coefficient and the effective mass, which can possibly be attributed to the formation of additional resonant states near Fermi level. Though the power factor does not improve, the significant reduction in the electronic part of the thermal conductivity leads to a measurable improvement in *ZT*.

Keywords: thermoelectric; misfit layer sulfide; spark plasma sintering; electrical conductivity; thermal conductivity

1 Introduction

Thermoelectric (TE) materials, which convert waste heat into electricity, are considered a promising way to save energy. The performance of thermoelectric materials is evaluated by a dimensionless parameter—the figure of merit *ZT,* which is given by $ZT = S^2\sigma T/\kappa$, where *T*, *S*, σ and κ are the absolute temperature, Seebeck coefficient, electrical conductivity and thermal conductivity, respectively. Finding promising low-cost thermoelectric materials with high *ZT* value, which are naturally abundant and able to operate well beyond room temperature, has been a challenge for thermoelectric researchers [1–3].

TiS_2 is a narrow-band-gap semiconductor with metallic conduction properties. It consists of layers of face-sharing TiS_6 octahedra with strong covalent

* Corresponding author.
E-mail: koumoto@apchem.nagoya-u.ac.jp

interaction and weak van der Waals forces between TiS_2 layers. TiS_2 has shown its potential as a promising thermoelectric material through its high power factor ($S^2\sigma$) at room temperature [4]. However, its TE performance is limited by its high thermal conductivity, so *ZT* value is not optimal [5–8]. The intercalation of bismuth sulfide (BiS) as a phonon barrier layer in van der Waals gaps to form $(BiS)_{1.2}(TiS_2)_2$ had become an effective way of reducing the thermal conductivity. However, reducing the thermal conductivity in this manner does not increase the value of *ZT*; electron transfer from BiS layers to TiS_2 layers increases the carrier concentration, thereby increasing the electrical conductivity and electronic thermal conductivity. As a result of this phenomenon, Seebeck coefficient decreases and the power factor cannot be optimized; moreover, the total thermal conductivity is not sufficiently suppressed [9,10].

In our previous work, we have substituted several electron acceptor dopants of alkaline earth (AE) into the titanium sites in TiS_2 layers and the bismuth sites in BiS layers [11]. All dopants effectively suppressed carrier concentration, greatly decreasing the electrical conductivity. However, unexpectedly Seebeck coefficient decreases despite of the reduction of carrier concentration, which we attributed to the lower effective mass and non-parabolic band structure. In this work, we have successfully found an acceptor dopant, chromium, which can enhance the effective mass and Seebeck coefficient, while decreasing carrier concentration. Though the power factor did not improved as a result, the significant reduction in the electronic part of the thermal conductivity led to a measurable improvement in *ZT* value.

2 Experiment

The sample preparation procedure has been reported in our previous work [11]. All pellets obtained from spark plasma sintering (SPS) have relatively high density of over 96%. We measured thermoelectric properties along the direction perpendicular to the pressure applied during the sintering process. XRD measurements helped to analyze the phase composition (RINT-2100, Rigaku). The ionic state of chromium was analyzed via XPS (JEOL, Al Kα source). The electrical conductivity and Seebeck coefficient were measured simultaneously by a four-probe method and a conventional steady-state method, in an Ar atmosphere (RZ-2001K, Ozawa Science). The thermal diffusivity and heat capacity were measured by laser-flash method (TC-9000V, ULVAC-RIKO) and differential scanning calorimetry (DSC-2910, TA Instruments), respectively. We also carried out Hall effect measurement in order to verify the carrier concentration by van der Pauw method (ResiTest 8300, Toyo Technica). Finally, the speed of sound was measured by ultrasonic pulse-echo method (Model 5800 PR, Olympus) at room temperature.

3 Results and discussion

Figure 1 shows that pure $(BiS)_{1.2}(TiS_2)_2$ has a natural superlattice structure, in which double TiS_2 layers and one BiS layer stack alternatively in the *c*-axis direction. Cr^{3+} (0.63 Å) was intended as a substitute at the Ti^{4+} (0.68 Å) site, rather than the Bi^{3+} (0.96 Å) site. XRD patterns of the pellets were observed in the direction perpendicular to the applied pressure during the sintering process and are shown in Fig. 2(a). Several

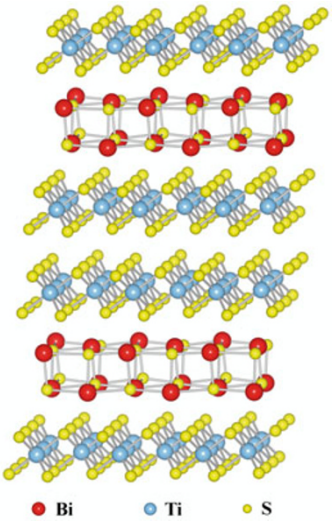

Fig. 1 The natural superlattice structure of $(BiS)_{1.2}(TiS_2)_2$ misfit layer sulfide.

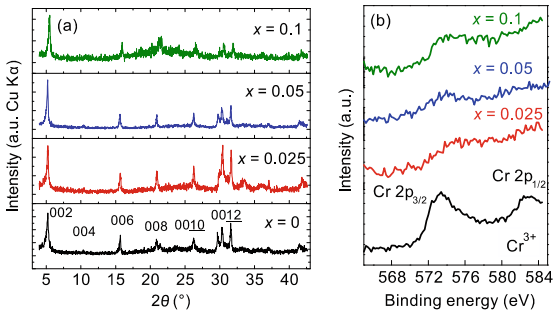

Fig. 2 (a) XRD pattern; (b) XPS spectra for $(BiS)_{1.2}(Ti_{1-x}Cr_xS_2)_2$ (x = 0, 0.025, 0.05 and 0.1).

strong peaks demonstrate that all the samples have high degree of (00*l*) orientation [9]. The peaks of chromium-doped misfit layer sulfides (x = 0.025, 0.05, 0.1) correspond to those of the undoped (x = 0) sample, proving that the chromium-doped misfit layer sulfide $(BiS)_{1.2}(Ti_{1-x}Cr_xS_2)_2$ has a crystal structure related to that of $(BiS)_{1.2}(TiS_2)_2$. No substantial changes were observed in the XRD pattern of the chromium-substituted compound, with only a slight shift to higher angles at around 27° (00$\underline{10}$), indicating that the layer spacing c in the doped misfit layer sulfide was shortened linearly from 16.9665 Å to 16.6849 Å, as the doping level x increased from 0 to 0.1.

Furthermore, we have performed XPS measurement to identify the ionic state of the chromium dopant. Figure 2(b) shows the XPS spectra of all doped samples. As a reference standard for Cr^{3+}, we also measured Cr^{3+} sulfide (Cr_2S_3); its XPS spectrum is shown in the lower part of the figure. The Cr $2p_{3/2}$ spectrum is shown for reference, at a binding energy (BE) of 573 eV. The peak positions of samples with chromium concentrations of x = 0.05 and 0.1 are quite similar to that of Cr^{3+} in Cr_2S_3, which implies that the chromium is nearly trivalent [12,13]. This proves that Cr^{3+} has been successfully substituted into Ti^{4+} octahedral sites in TiS_2 layers.

Figure 3 shows that chromium doping into titanium sites in TiS_2 layers significantly reduces the electrical conductivity in the whole temperature range studied. The decrease in electrical conductivity is in agreement with the increase in chromium doping levels. Furthermore, all compounds depicting this kind of change in electrical conductivity are metallic conductors [14–16]. The electrical conductivity of a material is determined by its carrier concentration and mobility. Therefore, we have carried out Hall measurements to examine carrier concentrations, so as to clarify the decrease in electrical conductivity. The carrier concentration of all samples decreased, as shown in Fig. 6. These results confirm that chromium doping reduces carrier concentration, which is consistent with the change in electrical conductivity of the samples.

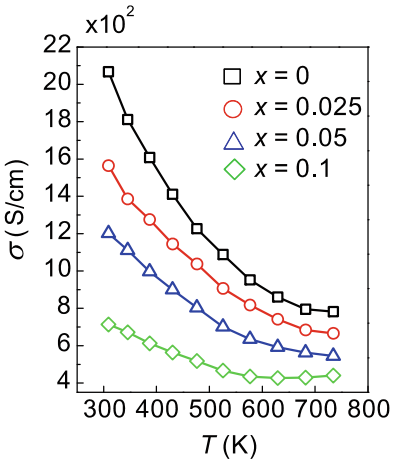

Fig. 3 The electrical conductivity of $(BiS)_{1.2}(Ti_{1-x}Cr_xS_2)_2$ (x = 0, 0.025, 0.05 and 0.1).

Figure 4 shows the temperature dependence of Hall mobility. The mobility for x = 0 has a temperature dependence proportional to $T^{-1.445}$, indicating the dominance of electron scattering by acoustic phonons [17–19]. However, increasing the chromium doping amount leads to a decrease in the dependence of Hall mobility on temperature. This implies that, in addition to acoustic phonon scattering, ionized impurity scattering or alloy scattering also takes place [20,21].

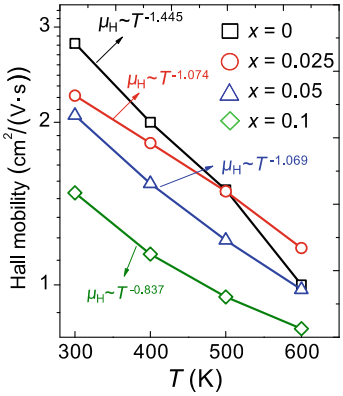

Fig. 4 Hall mobility of $(BiS)_{1.2}(Ti_{1-x}Cr_xS_2)_2$ (x = 0, 0.025, 0.05 and 0.1).

The samples show negative Seebeck coefficients, meaning that electrons are the main carriers, as shown in Fig. 5(a). The samples with chromium doping show higher Seebeck coefficients. The general expression for Seebeck coefficient is as follows [2]:

$$S = \frac{8\pi^2 k_B^2}{3eh^2} m^* T \left(\frac{\pi}{3n}\right)^{2/3} \quad (1)$$

where n is the carrier concentration, m^* is the effective mass of the carrier, k_B is Boltzmann constant (1.381×10^{-23} J/K), h is Plank constant (6.626×10^{-34} m^2·kg/s), e is the electron charge (1.602×10^{-19} C), and T is the temperature (K).

The increase in Seebeck coefficient with chromium doping is mainly due to the decrease in the carrier concentration n. Moreover, we should also point out that the effective mass shows a systematic increase

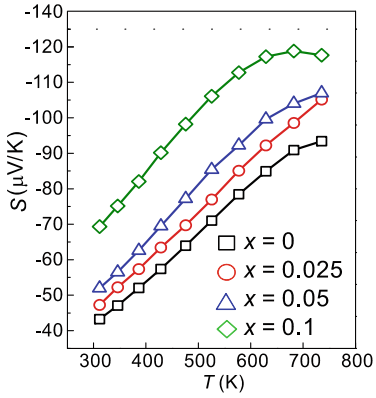

(a)

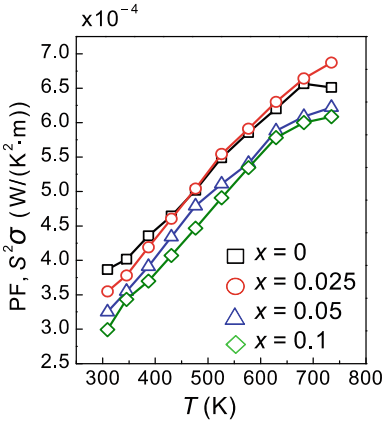

(b)

Fig. 5 (a) Seebeck coefficient; (b) power factor of $(BiS)_{1.2}(Ti_{1-x}Cr_xS_2)_2$ (x = 0, 0.025, 0.05 and 0.1).

with increasing doping levels, which further contributes to the increase in Seebeck coefficient, as shown in Fig. 6. This is different from our previous study, in which the alkaline earth metal doping ($(BiS)_{1.2}(Ti_{0.95}Mg_{0.05}S_2)_2$, $(Bi_{0.9}Ca_{0.1}S)_{1.2}(TiS_2)_2$ and $(Bi_{0.9}Sr_{0.1}S)_{1.2}(TiS_2)_2$) decreased the effective mass. It is believed that pure $(BiS)_{1.2}(TiS_2)_2$ has a non-parabolic band structure, so the decrease in carrier concentration can reduce the effective mass [22,23]. In the case of chromium doping, however, the effective mass increases as the decreasing of the carrier concentration, which may be due to the formation of additional states near Fermi level. Further investigation is needed to prove this assumption.

Figure 5(b) depicts the power factor calculated from their measured electrical conductivity and Seebeck coefficient. It shows that chromium doping cannot optimize the power factor due to the large decrease in electrical conductivity despite of the higher Seebeck coefficient.

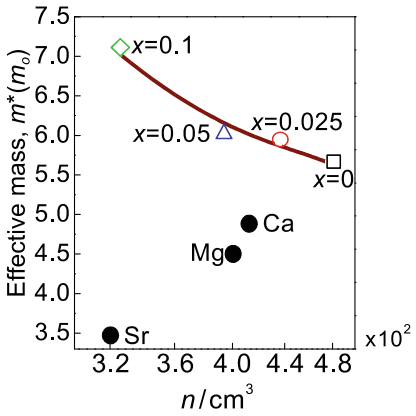

Fig. 6 The change in effective mass as a function of carrier concentration.

The total thermal conductivity (κ) can be expressed as the sum of the electronic thermal conductivity (κ_e) and the lattice thermal conductivity (κ_l): $\kappa = \kappa_e + \kappa_l$. The electronic thermal conductivity can be estimated from Wiedemann–Franz law, given by $\kappa_e = \sigma LT$, where L is Lorentz number for free electrons (2.44×10^{-8}/(J·C·K)^2), T is the temperature in K, and σ is the electrical conductivity. Subsequently, κ_l can be calculated from κ and κ_e [24,25]. Figure 7 shows

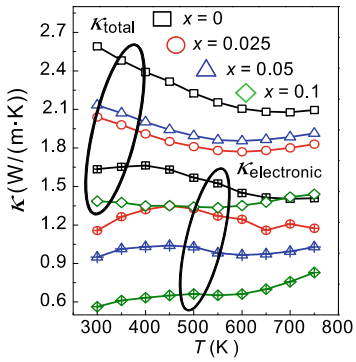

(a)

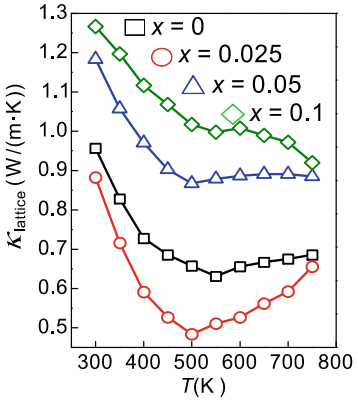

(b)

Fig. 7 Thermal conductivity: (a) the total thermal conductivity; (b) the lattice thermal conductivity of $(BiS)_{1.2}(Ti_{1-x}Cr_xS_2)_2$ (x = 0, 0.025, 0.05 and 0.1).

the thermal conductivity for all the samples with different chromium doping levels. Note that the total thermal conductivity of chromium-doped samples decreases in the whole temperature range. This significant decrease is mainly due to the decrease in electronic thermal conductivity, as shown in Fig. 7(a).

Note that in the case of $(BiS)_{1.2}(TiS_2)_2$, κ_e contributes more to κ than κ_l. This is also the case for $x = 0.025$ sample. However, for the samples with $x = 0.05$ and 0.1, the situation differs from that of the previous samples. Furthermore, chromium doping leads to different effects on the lattice thermal conductivity of the samples, as shown in Fig. 7(b). The samples with $x = 0.05$ and 0.1 show an increase in lattice thermal conductivity. This enhancement is probably due to a new structural ordering as a result of eliminating of planar stacking faults [10]. The resulting ordered structure should have weaker phonon scattering than the disordered $(BiS)_{1.2}(TiS_2)_2$ with planar stacking faults, and thus should have enhanced lattice thermal conductivity [26,27]. On the other hand, κ_l for the sample with $x = 0.025$ decreases due to the absence of structural ordering; as a result, this sample could have lower total thermal conductivity compared to the samples with $x = 0.05$ and 0.1.

The sound velocity measurement was carried out to examine the effect of structural ordering formation on the lattice thermal conductivity. The misfit layer sulfide has three polarization modes of sound velocity—one longitudinal mode and two transverse modes. The longitudinal mode (V_L) was measured along the pressure direction during densification; this mode has a correlation with the chemical bonding and the density of the samples. An increase in chemical bonding and density will decrease V_L and vice versa. The two transverse modes are along the y–z (V_{T1}) and x–y (V_{T2}) axes. V_{T1} is mainly determined by the interlayer bonding, while V_{T2} is determined by the intralayer bonding [9].

Table 1 shows that V_L had different values for each doping level, attributed to the different values of density. V_{T1} and V_{T2} of the samples with $x = 0.05$ and 0.1 increased, while for the $x = 0.025$ sample they decreased. The increase of V_{T1} in the samples with $x = 0.05$ and 0.01 was predicted to be due to the strengthening of the covalent bonding between chromium atoms and sulfur atoms within TiS_2 layers. The increase in V_{T2} is thought to be due to the reinforced intralayer bonding, and as a result the lattice thermal conductivity is enhanced. On the contrary, V_{T1} and V_{T2} of the $x = 0.025$ samples decreased due to the softening of the interlayer bonding and the weakening of the intralayer bonding, and as a result, the lattice thermal conductivity decreased [26].

Table 1 Density, V_L, V_{T1} and V_{T2} of $(BiS)_{1.2}(Ti_{1-x}Cr_xS_2)_2$ samples

Sample	ρ (g/cm^3)	V_L (m/s)	V_{T1} (m/s)	V_{T2} (m/s)
$x = 0$	4.4	3596	1396	1660
$x = 0.025$	4.2	3860	1375	1580
$x = 0.05$	4.4	3515	1502	1693
$x = 0.1$	4.3	3580	1698	1931

Figure 8 shows the ZT value calculated from the measured electrical conductivity, Seebeck coefficient and thermal conductivity. All chromium-doped samples exhibit an increase in ZT of 0.24–0.3 at a temperature of 750 K. Although the chromium substitution did not result in higher power factor, its low total thermal conductivity contributed to an increase in ZT.

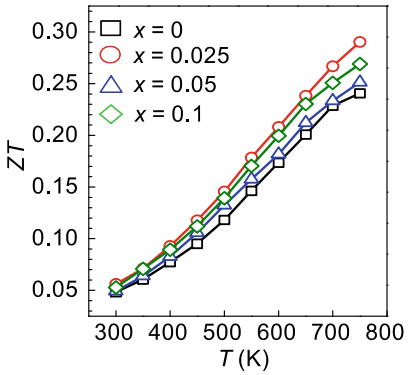

Fig. 8 The dimensionless figure of merit ZT for $(BiS)_{1.2}(Ti_{1-x}Cr_xS_2)_2$ ($x = 0$, 0.025, 0.05 and 0.1).

4 Summary

In this work, we have successfully improved the thermoelectric properties of $(BiS)_{1.2}(TiS_2)_2$ misfit layer sulfide through the optimization of carrier concentration by chromium doping. The chromium ions substituted for the titanium sites reduced the carrier concentration and increased Seebeck coefficient. Unlike other acceptor dopants, chromium increased the effective mass, which further enhanced Seebeck

coefficient. It is assumed that additional resonant states may be formed near Fermi level which can account for the increase in effective mass. The electronic thermal conductivity was significantly reduced due to the decrease in electrical conductivity. Consequently, the overall *ZT* value was measurably improved, even though the power factor decreased slightly.

It is still unclear why chromium doping can enhance the effective mass of $(BiS)_{1.2}(TiS_2)_2$ misfit layer compound, while many other cationic doping such as alkaline earth elements and other transition metal elements even decrease it. It is assumed that the formation of impurity band or resonant states near Fermi level can be responsible for the increase of the effective mass in chromium-doped sample. We realized that further investigation, such as DFT calculation or measurement of low temperature heat capacity, is required to better understand the alteration of density of states (DOS).

Acknowledgements

The authors thank Prof. Saki Sonoda from Kyoto Institute of Technology (KIT) for her generous advice.

References

[1] Pei YZ, Shi XY, LaLonde A, *et al*. Convergence of electronic bands for high performance bulk thermoelectrics. *Nature* 2001, **473**: 66–69.

[2] Snyder GJ, Toberer ES. Complex thermoelectric materials. *Nat Mater* 2008, **7**: 105–114.

[3] Hicks LD, Dresselhaus MS. Effect of quantum-well structures on the thermoelectric figure of merit. *Phys Rev B* 1993, **47**: 12727–12731.

[4] Imai H, Shimakawa Y, Kubo Y. Large thermoelectric power factor in TiS_2 crystal with nearly stoichiometric composition. *Phys Rev B* 2001, **64**: 241104-1–241104-4.

[5] Slack GA. New materials and performance limits for thermoelectric cooling. In *CRC Handbook of Thermoelectric*. Rowe DM, Ed. Boca Raton, FL, USA: CRC Press, 1995: 407–440.

[6] Chen CH, Fabian W, Brown FC, *et al*. Angle-resolved photoemission studies of the band structure of $TiSe_2$ and TiS_2. *Phys Rev B* 1980, **21**: 615–624.

[7] Wilson JA. Modelling the contrasting semimetallic characters of TiS_2 and $TiSe_2$. *Phys Status Solidi b* 1978, **86**: 11–36.

[8] Guilmeau E, Bréard Y, Maignan A. Transport and thermoelectric properties in copper intercalated TiS_2 chalcogenide. *Appl Phys Lett* 2011, **99**: 052107.

[9] Wan CL, Wang YF, Wang N, *et al*. Low-thermal-conductivity $(MS)_{1+x}(TiS_2)_2$ (M = Pb, Bi, Sn) misfit layer compounds for bulk thermoelectric materials. *Materials* 2010, **3**: 2606–2617.

[10] Wan CL, Wang YF, Wang N, *et al*. Layer-structured metal sulfides as novel thermoelectric materials. In *Modules, Systems and Applications in Thermoelectrics*. Rowe DM, Ed. Boca Raton, FL, USA: CRC Press, 2012: 4.1–4.11.

[11] Putri YE, Wan CL, Wang YF, *et al*. Effects of alkaline earth doping on the thermoelectric properties of misfit layer sulfides. *Scripta Mater* 2012, **66**: 895–898.

[12] Ünveren E, Kemnitz E, Hutton S, *et al*. Analysis of highly resolved X-ray photoelectron Cr 2p spectra obtained with a Cr_2O_3 powder sample prepared with adhesive tape. *Surf Interface Anal* 2004, **36**: 92–95.

[13] Biesinger MC, Brown C, Mycroft JR, *et al*. X-ray photoelectron spectroscopy studies of chromium compounds. *Surf Interface Anal* 2004, **36**: 1550–1563.

[14] Zhang J, Qin XY, Xin HX, *et al*. Thermoelectric properties of Co-doped TiS_2. *J Electron Mater* 2011, **40**: 980–986.

[15] Dingle R, Störmer HL, Gossard AC, *et al*. Electron mobilities in modulation-doped semiconductor heterojunction superlattices. *Appl Phys Lett* 1978, **33**: 665–667.

[16] Seto JYW. The electrical properties of polycrystalline silicon films. *J Appl Phys* 1975, **46**: 5247–5254.

[17] Sze SM. *Semi Conductor Devices*. 2nd edn. USA: Wiley, 2001.

[18] Wiegers GA. Charge transfer between layers in misfit layer compounds. *J Alloys Compd* 1995, **219**: 152–156.

[19] Debye PP, Conwell EM. Electrical properties of *N*-type germanium. *Phys Rev* 1954, **93**: 693–706.

[20] Tichý L, Frumar M, Kincl M, *et al*. Mixed scattering mechanism of free current carriers in $SnBi_4Te_7$ single crystals. *Phys Status Solidi a* 1981,64: 461–466.

[21] Flage-Larsen E, Prytz Ø. The Lorenz function: Its properties at optimum thermoelectric figure-of-merit**.** *Appl Phys Lett* 2011, **99**: 202108.

[22] Sofo JO, Mahan GD. Electronic structure of $CoSb_3$: A narrow-band-gap semiconductor. *Phys Rev B* 1998, **58**: 15620–15623.

[23] Wu J, Walukiewicz W, Shan W, *et al*. Effects of the narrow band gap on the properties of InN. *Phys Rev B* 2002, **66**: 201403-1–201403-4.

[24] Zhang J, Qin XY, Li D, *et al*. The transport and thermoelectric properties of Cd doped compounds $(Cd_xTi_{1-x})_{1+y}S_2$. *J Alloys Compd* 2009, **479**: 816–820.

[25] Minnich AJ, Dresselhaus MS, Ren ZF, *et al*. Bulk nanostructured thermoelectric materials: Current research and future prospects. *Energy Environ Sci* 2009, **2**: 466–479.

[26] Wan CL, Wang YF, Norimatsu W, *et al*. Nanoscale stacking faults induced low thermal conductivity in thermoelectric layered metal sulfides. *Appl Phys Lett* 2012, **100**: 101913-1–101913-4.

[27] Cahill DG, Watson SK, Pohl RO. Lower limit to the thermal conductivity of disordered crystals. *Phys Rev B* 1992, **46**: 6131–6140.